

Physical properties of CeIrSi with trillium lattice frustrated magnetism

F. Kneidinger¹, I. Zeiringer², A. Siderenko¹, E. Bauer¹, H. Michor¹, P. Rogl², J.G. Sereni³

¹ *Institute of Solid State Physics, TU Wien, A-1040 Wien, Austria*

² *Institut fuer Physikalische Chemie, Universitaet Wien, A-1020 Wien, Austria*

³ *Low Temperature Division CAB-CNEA, CONICET, 8400 S.C. de Bariloche, Argentina*

(Dated: November 28, 2021)

Magnetic (χ), transport (ρ) and heat capacity (C_m) properties of CeIrSi are investigated to elucidate the effect of geometric frustration in this compound with trillium type structure because, notwithstanding its robust effective moment, $\mu_{\text{eff}} \approx 2.46\mu_B$, this Ce-lattice compound does not undergo a magnetic transition. In spite of that it shows broad $C_m(T)/T$ and $\chi(T)$ maxima centered at $T_{\text{max}} \approx 1.5$ K, while a $\rho \propto T^2$ thermal dependence, characteristic of electronic spin coherent fluctuations, is observed below $T_{\text{coh}} \approx 2.5$ K. Magnetic field does not affect significantly the position of the mentioned maxima up to ≈ 1 T, though $\chi(T)$ shows an incipient structure that completely vanishes at $\mu_0 H \approx 1$ T. Concerning the $\rho \propto T^2$ dependence, it is practically not affected by magnetic field up to $\mu_0 H = 9$ T, with the residual resistivity $\rho_0(H)$ slightly decreasing and $T_{\text{coh}}(H)$ increasing. These results are compared with the physical properties observed in other frustrated intermetallic compounds.

I. INTRODUCTION

The lack of magnetic order in lattice arrangements of robust magnetic moments allows to access to exotic ground states with high density of low energy excitations. Two typical scenarios allow to prevent the development of magnetic order: i) the weakness of the magnetic interactions or ii) the frustration of antiferromagnetic interactions. In the former, cerium magnesium nitrate hydrate (CMN) is the exemplary case because it remains paramagnetic down to ≈ 2 mK due to the large Ce-Ce spacing $d_{\text{Ce-Ce}} \approx 11$ Å [1] and the absence of conduction electrons. In the latter context, two circumstances may produce frustration; one due to geometrical constraints like triangular (2D) or tetrahedral (3D) spin lattices, or because of the competition between nearest (nn) and next nearest neighbors (nnn) interactions [2]. The pyrochlore structure of the $\text{Dy}_2\text{Ti}_2\text{O}_7$ spin-ice [3] is an exemplary system for the 3D-tetrahedral coordination case, whereas some 2-2-1 [4] compounds showing a network of triangles and squares exhibit magnetic frustration in their basal (2D) planes. Finally, the competition between 'nn' and 'nnn' interactions can be exemplified by Yb_4LiGe_4 [5].

Among the crystalline structures favoring 3D geometric frustration, the cubic trillium (LaIrSi-type) structure [6–8] should provide an ideal playground for a study of the competition between RKKY interactions and frustration effects. Several light rare earth - iridium - silicides (REIrSi, RE = rare earth) are members of this structure type.

Ternary intermetallics REIrSi have been intensely studied in the past few decades. The respective crystal structure depends on the distinct

rare earth element. Compounds with RE = La, Ce, Pr and Nd exhibit the cubic LaIrSi structure type (space group $P2_13$) [6, 7], where inversion symmetry is missing. This structure type is a ternary ordered version of the binary SrSi_2 type (space group $P4_132$). Due to ordering of the Ir and Si atoms in LaIrSi, symmetry is lowered, as evidenced from the respective space groups. The iridium and silicon atoms build up a three-dimensional [IrSi] network with rather short Ir-Si distances, inferring strong covalent bonding [8]. On the other hand, distances of between rare earth ions and Si or Ge are much larger, evidencing a much weaker bonding [8].

Silicides with heavy rare earth elements (RE from Gd to Lu), however, crystallizing in the orthorhombic TiNiSi structure (space group $Pnma$) [9]. The same is true for ScIrSi and YIrSi. In this structure, the iridium and silicon atoms form a three-dimensional [IrSi] network in which the heavy rare earth atoms are located in distorted hexagonal channels. Short Ir-Si distances are indicative for strong Ir-Si bonding [10]. The Sm based compound with an empirical formula $\text{SmIr}_{0.266}\text{Si}_{1.734}$ is found in the tetragonal $\alpha\text{-ThSi}_2$ structure type, space group $I4_1/amd$.

For LaIrSi, a superconducting phase transition at $T_c = 2.3$ K has been obtained in Ref. [7]. A subsequent study by Evers et al. [11] revealed superconductivity below $T_c = 1.5$ K. Upon annealing, this temperature shifted up to 2.3 K. The authors, however, concluded from just a small anomaly at $T = T_c$ that superconductivity in this compound is not a bulk property. The authors of the present study (compare Ref. [12]) also have not observed bulk superconductivity, as evidenced from missing an appropriate jump in the heat capacity data and from the non-zero resistance at 350 mK.

While CeIrSi was characterised from tempera-

ture dependent susceptibility data as a paramagnet without magnetic ordering down to 1.5 K [8], for NdIrSi, Chevalier et al. [7] reported a ferromagnetic ground state below $T_C = 10$ K from a spontaneous magnetisation. This, in addition, was supported from a positive value of the paramagnetic Curie temperature ($\theta_p = 12$ K). The study by Heying et al. [8] confirmed the LaIrSi crystal structure for PrIrSi, too, but no physical properties were reported.

Magnetic properties and magnetic structures of REIrSi (RE from Tb to Er) were revealed by Szytula et al. [13]. Sine modulated and collinear antiferromagnetic orders at lower temperatures have been derived in this study from elastic neutron scattering experiments.

Within the series REIrSi (RE = Gd, Ho, Er, Yb, Lu), the unit cell volume decreases monotonically from GdIrSi to YbIrSi [8]. This would infer the magnetic $4f^{13}$ electronic configuration of the Yb ion in this ternary compound. Thus, paramagnetic behaviour is expected [10]. A temperature independent susceptibility evidences Pauli paramagnetism for LuIrSi [8].

In the present study we aim a thorough characterisation of CeIrSi in the context of the LaIrSi crystal structure. Because of distinct features of the trillium structure, a weaker Ce-Ce connectivity with the next nearest neighbours is expected, compared to cases with the pyrochlore structure, as it forms a three-dimensional network of corner-sharing triangles (resembling a trillium flower, see Fig. 1) instead of corner-sharing tetrahedra. Within this peculiar structure the 6 Ce nearest neighbours are at $d_{Ce-Ce} = 3.855(1)$ Å [8], which is close to a direct Ce-Ce contact. In this work structural, thermodynamic and transport properties of CeIrSi are investigated to elucidate the effect of geometric frustration with respect to ground state properties of this compound.

II. EXPERIMENTAL DETAILS

A. Sample preparation and characterization

Polycrystalline samples of LaIrSi and CeIrSi were obtained by melting pure ingots of respective components weighted in proper stoichiometric composition in an arc furnace with argon atmosphere, using Ti as getter material. Several remelting processes were carried out to assure sample homogeneity. Subsequently, the samples were sealed in quartz tubes and annealed for one week. X-ray powder diffraction (XRD), scanning electron microscopy (SEM) and electron probe micro analysis

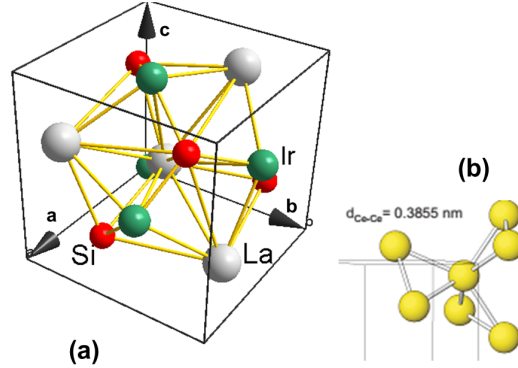


FIG. 1. (Color online) LaIrSi crystal structure type in two coordination representations, a) with ligand atoms and b) with La next neighbors.

(EPMA) were used for the characterization of the samples.

As a derivative of the non-centrosymmetric SrSi₂-type structure [6], LaIrSi and CeIrSi compounds were found to have respective lattice parameters: $a = 6,3766(3)$ Å and $6,2951(1)$ Å. The actual relative concentration was determined by EPMA as: 33.4; 34.7; 31.9% for LaIrSi and 34.3; 32.7; 33.0% for CeIrSi. The LaIrSi sample contains small amounts (< 2%) of LaIr₂Si₂ as an impurity phase, and CeIrSi also contains about 2% of CeIr₂Si₂, CeSi_{1.7} and small amounts of cerium oxide as impurities.

B. Magnetic, transport and thermal measurements

The temperature dependent magnetization was measured employing a Cryogenic superconducting quantum interference device (SQUID) magnetometer (S700X) at temperatures from 0.3 to 2 K with a ³He-insert and from 1.8 K to room temperature with standard ⁴He variable temperature insert and as a function of field up to 7 T.

Electrical resistivity measurements were performed employing a standard four probe configuration using an a.c. measurement method. Contact wires were made of gold, with a diameter of 50 μm respectively. Measurements were carried out down to 350 mK and magnetic fields up to 9 T.

Specific heat measurements were carried in a PPMS system using a He³ inset to reach 400 mK applying the relaxation time method below 20 K. For this purpose, samples were prepared as a cuboid with a base of up to 2.5 mm times 2.5

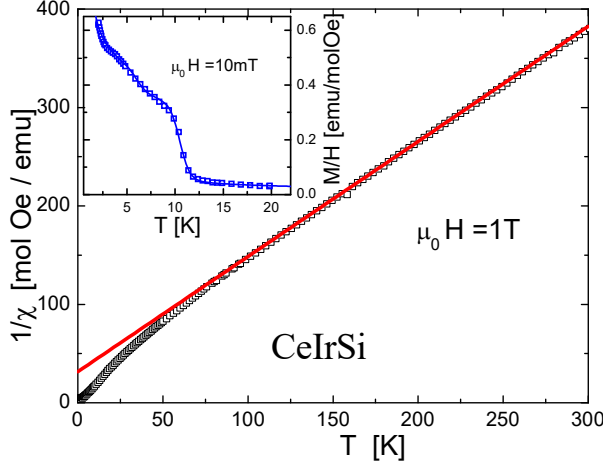


FIG. 2. (Color online) Inverse susceptibility, continuous curve represents the fit according to Eqn.(1). Inset: analysis of the spurious ferromagnetic contribution below 10 K, see the text.

mm. In general, a sample mass between 1 mg to 200 mg were mounted on the sample stage and attached with Apiezon N to the platform. Between $T = 20$ K and room temperature the He^3 inset was removed.

III. EXPERIMENTAL RESULTS

A. Magnetic Properties

1. Susceptibility

The high temperature dependent magnetic susceptibility (defined as $\chi = M/H$) in an applied field of 1 Tesla was measured between $T = 2$ K and room temperature. The results are properly described in terms of the Curie-Weiss (CW) law, including a temperature independent contribution, χ_P :

$$\chi(T) = C/(T + \theta) + \chi_P \quad (1)$$

Here the Curie constant $C \propto \mu_{eff}^2$, μ_{eff} is the effective magnetic moment, and θ_P the paramagnetic Curie-Weiss temperature.

The Curie-Weiss law allows to analyze the magnetic susceptibility $1/\chi$ in the paramagnetic temperature range. A least squares fit for $T \geq 75$ K according to Eq(1) is shown as a solid curve in Fig. 2, revealing that $\mu_{eff} = 2.53\mu_B$, in accordance to the value of a free Ce^{3+} ion. The paramagnetic Curie temperature was derived as $\theta_P = -21$ K, suggesting antiferromagnetic (AFM)

interactions among the Ce^{3+} ions, whereas the Pauli-like contribution was found to be quite small, $\chi_P = 1.3 \times 10^{-4}$ emu/mol Oe. These values are in good agreement with Ref. [8] that reports a similar downwards curvature of $1/\chi$, with $\mu_{eff} = 2.56(2)\mu_B$ and $\theta_P = -24(1)$ K. The small difference to the present results seems to be a result of the inclusion of the Pauli susceptibility χ_P in the data evaluation.

Below 60 K the inverse susceptibility significantly deviates from Curie-Weiss behavior, referring to the splitting of the $\text{Ce}^3 + J = 5/2$ Hund's ground state due to crystalline electric field effects. Around $T \approx 10$ K the onset of a spurious ferromagnetic (FM) signal becomes evident (inset, Fig. 2). Thus, the measured magnetic susceptibility at low temperature is described using two contributions: $M/H|_{meas} = M/H|_{bulk} + M/H|_{spur}$, where $M/H|_{bulk} = 0.33/(T - 0.3)$ and $M/H|_{spur} = 0.14 \times \tanh(10.6 - T) + 0.045 \times \text{atan}(6 - T) + 0.23$. The $M/H|_{bulk}(T)$ term represents the CW thermal dependence originated by the paramagnetic doublet GS, whereas $M/H|_{spur}(T)$ accounts for the mentioned FM contribution at $T < 11$ K and a weaker one at $T \approx 6$ K. This spurious component can be attributed to the formation of a CeSi_{2-x} (with $x \approx 0.2$) solid solution [14].

The low temperature magnetic susceptibility ($T < 2$ K) was measured below 2 K in applied fields from $\mu_0 H = 5$ mT up to 1 T. In Fig. 3a details of the temperature dependence of $M/H(T)$ is shown around the maximum at $T \approx 1.2$ K. A detailed analysis of the $M/H(T)$ maximum reveals a weak structure; the maximum remains nearly constant at $T \approx 1.25$ K until vanishing at $\mu_0 H \approx 200$ mT. Additionally, a kink in M/H decreases in temperature, from $T \approx 1$ K to $T < 0.5$ K at $\mu_0 H = 200$ mT. These features reveal a competition between two weak magnetic configurations which are quenched at relatively low field.

2. Magnetization

The isothermal field dependence of the magnetization, measured up to $\mu_0 H = 7$ T is included in Fig. 3b. Only a slight variation of M vs $\mu_0 H$ is observed between 0.5 and 2.15 K, in agreement with the results presented in Fig. 3a. The paramagnetic behavior can be recognized above the $T = 5.8$ K isotherm through the collapse of the M vs H/T curves (not shown). Strictly, isothermal curves for $T \leq 8.8$ K do not extrapolate to zero due to the spurious FM contribution, however its intensity is so low ($\approx 0.01\mu_B/\text{f.u.}$ at 0.5 K) that it cannot be appreciated in the field scale of Fig. 3b. Accord-

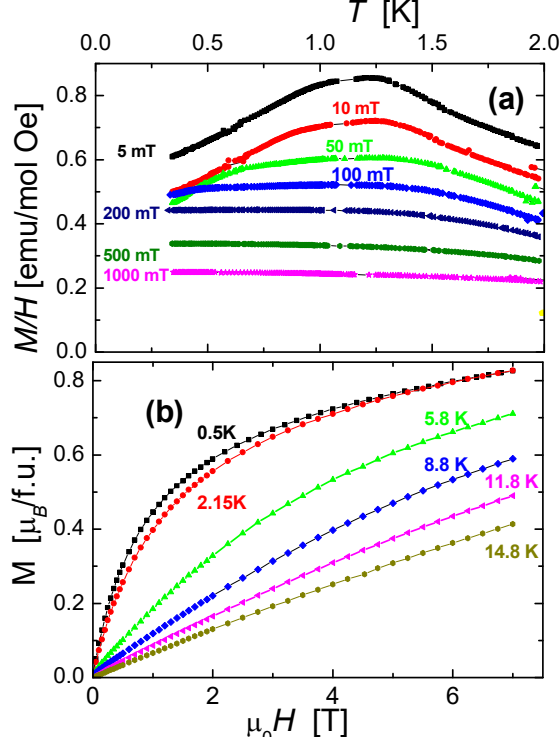


FIG. 3. (Color online) a) Low temperature magnetic susceptibility evaluated as $M/H(T)$ performed under relatively weak magnetic fields, the curves shifted by the effect of the FM contribution arising at $T < 11$ K. b) Low temperature magnetization measurements of CeIrSi.

ing to Fig. 3(b), the magnetization of CeIrSi at $T = 0.5$ K reaches $0.82\mu_B$ at 7 T, with a tendency of a further increase. The magnetic moment of Ce^{3+} in CeIrSi at low temperatures is derived from the respective wave function of the crystalline electric field (CEF) ground state. For $J = 5/2$ with respect to the cubic crystal structure of CeIrSi, a twofold (Γ_7) and a fourfold (Γ_8) degenerate state is originated. The magnetic moment associated with the doublet is calculated as $M(\Gamma_7) = 0.71\mu_B$, which is derived by $M_{\text{Ce}^{3+}} = g_L\mu_B \langle \Gamma_7 | J_z | \Gamma_7 \rangle = 6/7\mu_B(1/6 - 5/2 > +5/6|3/2 >) = 0.714\mu_B/\text{Ce-ion}$. The magnetic moment related to the quartet Γ_8 , however, is much larger. In conjunction with the so-called Van Vleck contribution, i.e., the non-diagonal element $\langle \Gamma_7 | J_z | \Gamma_8 \rangle$, the difference between the experimental data and the CEF magnetic moment might be explained.

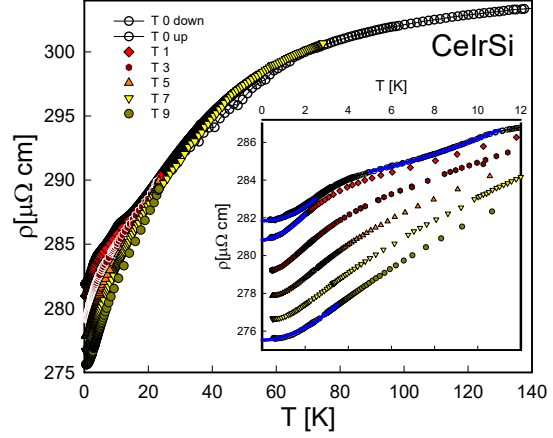


FIG. 4. (Color online) Temperature and field dependent electrical resistivity measurements of CeIrSi. The inset shows the low temperature range, from 0 to 12 K to reveal a coherent spin scattering.

B. Electrical Resistivity

Electrical resistivity measurements $\rho(T)$ at high temperature ($T > 140$ K) show a tendency to saturation slightly above $305 \mu\Omega \text{ cm}$ at room temperature, while from 100 K to 15 K the value decreases to $288 \mu\Omega \text{ cm}$, see Fig. 4. Apart from the linear phonon contribution to $\rho(T)$, the continuous thermal curvature can be associated to the progressive thermal population of the excited crystalline electric field level above the ground state. As explained above, the Ce $J = 5/2$ state in CeIrSi is split into a doublet and a quartet.

A weak kink in $\rho(T)$ around $T \approx 10.2$ K refers to the onset of long range magnetic order of ferromagnetic CeSi_{1.7}. The rather small signal change, however, indicates just a low volume fraction, which, in addition, becomes fully suppressed by rising magnetic fields (compare Fig. 4).

With decreasing temperature, the system enters into a coherent spin fluctuation regime below about 2.5 K, as evidenced by a T^2 temperature dependence of $\rho(T)$ (solid lines, inset, Fig. 4). This regime appears to be quite robust with respect to distinct changes observed in both $C_p(T)$ and $\chi(T)$ in this temperature range.

By increasing magnetic fields the Ce-spins get aligned along the external field direction and thus reduce the electrical resistivity. Notably, a negative residual magnetoresistivity $\rho_0(H)$ at $T \rightarrow 0$ shows an almost linear dependence with a small ratio $\Delta\rho_0/\Delta H \approx 0.7 \mu\Omega \text{ cm}/\text{T}$ and an expanding range of spin fluctuation type behaviour. This reveals a magnetic scattering component in ρ_0 that is

reduced by increasing magnetic field. On the other hand the influence of external magnetic fields up to 9 T appears to be negligible at temperatures above 60 K

C. Specific Heat

Specific heat measurements $C_P(T)$ provide a deeper insight on the GS nature of CeIrSi. Zero field measurements, performed from 1.9 K up to 80 K are shown in the inset of Fig. 5a. The magnetic specific heat contribution C_m was obtained by subtracting the phonon contribution C_{ph} extracted from the isotypic compound LaIrSi [12], i.e. $C_m = C_P - C_{ph}(\text{LaIrSi})$. At low temperature $C_P(\text{LaIrSi})$ can be described simply by $C_P(\text{LaIrSi}) = \gamma T + \beta T^3$ with $\gamma = 2.8 \text{ mJ/mol K}^2$ and $\beta = 0.672 \text{ mJ/mol K}^4$. In the inset of Fig. 5a, the specific heat is depicted for both compounds up to 90 K.

The FM transition of CeSi_{1.8} at $T \approx 10 \text{ K}$, weakly present in $\rho(T)$ measurements, is not observed in specific heat at all because of the small amount of the involved mass. The most relevant feature observed in Fig. 5a is the $C_m(T)/T$ maximum centered at $T^* \approx 1.5 \text{ K}$, that almost coincides in temperature with the maximum in the magnetic susceptibility as presented in detail in Fig. 6a. Notably, there is no distinct specific heat jump associated to the $C_m(T)/T$ maximum: the $T > T^*$ tail shows a long monotonous decrease. A comparison with theoretical predictions for a trillium-lattice system of spin ice type behavior, studied using Monte Carlo calculations [15], is included as a solid curve in Fig. 5a, after scaling the respective C_m/T^* values. Deviations from the measured thermal dependence can be due to the finite number (six) unit cells, that does not reproduce the continuous spectrum of excitations observed in the real system. At high temperature ($T \geq 10 \text{ K}$) there is an incipient contribution of the excited CEF levels, not included into the model.

An analysis of the GS and excited CEF levels contributions to specific heat up to 100 K is presented in Fig. 5b as $C_m(T)/T = C_{GS}/T + C_{CEF}/T$. As mentioned in subsection III-A, in a cubic symmetry the CEF splits the six fold degenerate $J = 5/2$ state into a doublet (Γ_7) and a quartet (Γ_8). Except for bcc structures, the former is the GS and the later the excited one, centered at the energy $k_B \Delta$. The $C_{CEF}(T)$ dependence is usually described by a standard Schottky type anomaly which, for such a level spectrum, reaches a maximum value of $C_{Sch}(T_{max}) = 6.3 \text{ J/mol K}$. This is not the case for CeIrSi be-

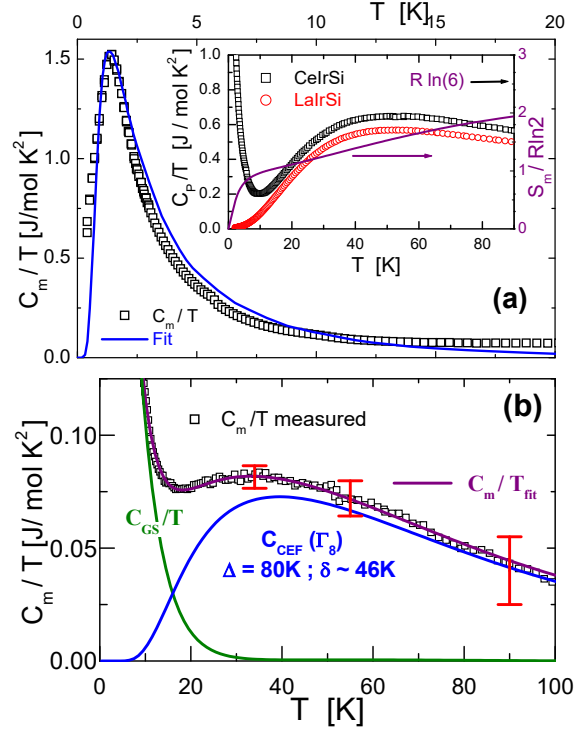


FIG. 5. (Color online) a) Low temperature magnetic contribution $C_m(T)/T$ up to 20 K and (continuous curve) comparison with theoretic prediction for a trillium-type lattice [15]. Inset: (left axis) measured specific heat $C_P(T)/T$ of CeIrSi and LaIrSi in a temperature range up to 90 K and (right axis) entropy variation $S_m(T)$ normalized to a doublet GS - $R \ln 2$. b) High temperature $C_m(T)/T$ of CeIrSi showing the analysis for GS and excited Γ_8 quartet contributions (see the text). Error bars are representative of the uncertainty of the $C_P(T)$ measurements.

cause $C_{Sch}(T_{max}) \approx 4.2 \text{ J/mol}$. This flattening of the anomaly can be attributed to a significant broadening of the excited Γ_8 quartet due to hybridisation of local and itinerant states. A simple approach to that scenario can be done by mimicking the mentioned broadening with a symmetric level distribution $\pm \delta_i$ around the nominal energy Δ , using the formula:

$$C_{CEF} = R \sum_i A_i \left[\left(\frac{\Delta \pm \delta_i}{2T} \right) / 2 \cosh \left(\frac{\Delta \pm \delta_i}{2T} \right) \right]^2 \quad (2)$$

where R is the gas constant and A_i a factor that accounts for the weight of each level. To describe some Lorentian distribution for the density of states distribution, the values: $A_1 = 1/2$, $A_2 = 1/4$ and $\delta_1 = 2 \times \delta_2$ are chosen. The model curve is compared with the experimental data in Fig. 5b, obtaining a very good fit up to 100 K. The

extracted values are $\Delta = 80$ K and $\delta_1 = 46$ K. The later allows an estimation of the effective Γ_8 broadening and consequently a scale for the Kondo energy. Such a rough evaluation of the parameters describing quartet energy and broadening confirms the pure doublet character of the GS, which is one of the main requirements for the following discussion concerning the low temperature behavior of this compound.

In order to check the proper distribution of respective level weights, the corresponding entropy gain, extracted from this levels scheme, was computed up to room temperature, where the expected $\Delta S_m(\Gamma_8) = R \ln(6/2)$ is asymptotically reached. However, by applying this entropic analysis to the GS doublet, an excess of about 10% of entropy was detected for the power law function describing the $C_{GS}(T)/T$ contribution at high temperature. This excess can be attributed to the fact that the power law function: $C_{GS}(T)/T = 6.5/(T^{1.7} + 2.1)$ used to describe the measured $C_m(T)/T$ data dependence below about 7 K (see for details the discussion in Subection IV-A and Fig. 7), does not describe the actual density of state of the physical system at higher temperature. To leave out this deviation, we have introduced a cut-off at about 20 K, with the purpose to progressively suppress the high temperature tail. This objective was reached by subtracting a Schottky type anomaly which has a continuous increase up to a characteristic energy and a high temperature tail approaching the power low temperature dependence. The thermal energy of this cut-off was tuned such to reach the expected value of $S_{GS} = R \ln 2$ at high temperature.

IV. DISCUSSION

A comparison between $\chi(T)$, $C_m(T)/T$ and $\rho(T)$ is presented in Fig. 6a. Notably both $\chi(T)$ and $C_m(T)/T$ maxima, centered between $T_{max} = 1.3$ and 1.5 K respectively, occur within the range at which $\rho(T) \propto T^2$. Together with the lack of a $C_m(T)/T$ jump, this behavior excludes $\chi(T)$ and $C_m(T)/T$ maxima as due to a standard phase transition. To gain insight into the magnetic character of the GS, we have performed specific heat measurements under magnetic fields up to $\mu_0 H = 8$ T, see Fig. 6b. The maximum of $C_m(T, H)/T$ decreases and slightly shifts to higher temperature up to $\mu_0 H \approx 2$ T. The solid line in Fig. 6b describes the evolution of the maximum, which broadens once the applied field starts to polarize the GS spins above $\mu_0 H \approx 4$ T.

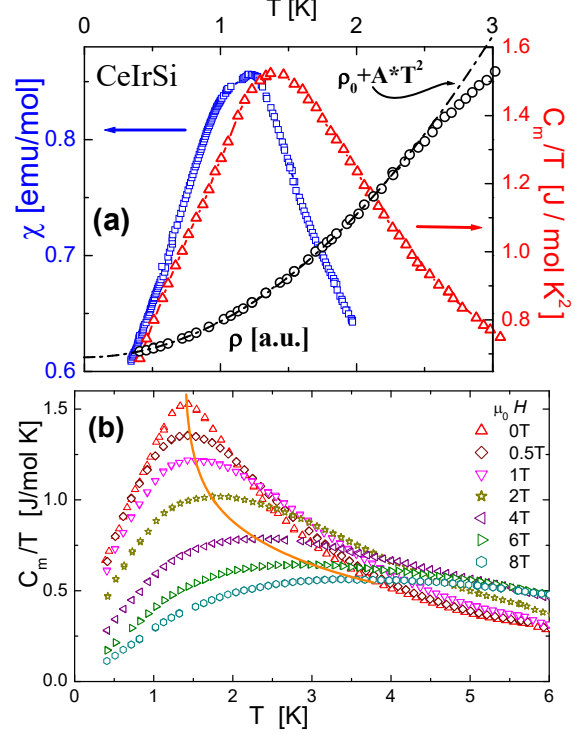


FIG. 6. (Color online) a) Comparison between $\chi(T)$, $C_m(T)/T$ and $\rho(T)$ at $T < 3$ K. b) Specific heat dependence of CeIrSi in magnetic field up to $\mu_0 H = 8$ T. Continuous curve: guide to the eyes tracing the $C_m(T, H)/T$ maxima.

A. Entropy trajectory and magnetic frustration

In order to analyze the nature of the low temperature anomaly presented in Fig. 6, one may compare this behavior with similar ones observed in other intermetallics [18]. A common feature of those systems is the power law thermal dependence of $C_m(T)/T$ above its maximum. In Fig. 7 this feature is verified in a double logarithmic representation, where the measured values are accounted for by a modified power law, $C_{fit}/T = 6.5/(T^{1.7} + 2.1)$. Such a thermal dependence is comparable with that observed in compounds recognized as frustrated systems [18]. Differently from those recognized as spin glasses, with a $C_m(T) \propto 1/T^2$ tail at high temperature, one notices that the present fitted power law dependence holds up very close to the maximum with a clearly different exponent: 1.7, instead of 3 for the spin glass in a $C_m(T)/T$ representation. Furthermore, the $\rho \propto T^2$ dependence observed in this compound is not the expected for a spin glass [19]

In frustrated systems, the $C_m(T)/T$ maxi-

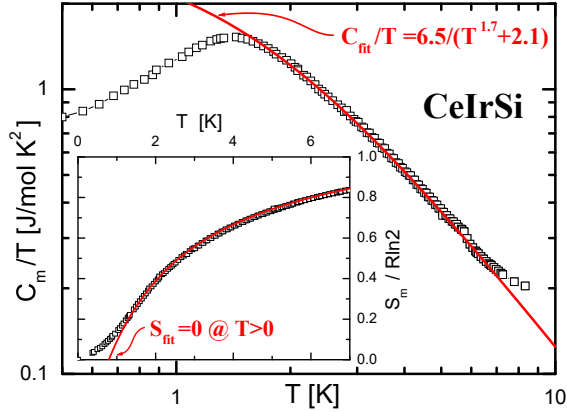


FIG. 7. (Color online) Double logarithmic representation showing the thermal dependence of $C_m(T)/T$ above the maximum and the corresponding power law fit (solid curve). Inset: thermal dependence of the Entropy compared with the extrapolation of $S_{fit}(T)$ to zero (solid line) at finite temperature.

mum was associated to the temperature at which the thermal trajectory, represented by $C_{fit}(T > T_{max})/T$ in Fig. 7 as a solid curve, changes because of thermodynamic constraints. If $C_m(T)/T$ followed the trajectory described by $C_{fit}(T < T_{max})/T$ (solid red line in Fig. 7) it would reach unphysical values at $T \rightarrow 0$. As a consequence, the entropy evaluated as $S_{fit} = \int C_{fit}/T dT$ would exceed the available degrees of freedom ($R \ln 2$) for a doublet ground state.

An alternative description can be done analyzing the actual trajectory of the entropy shown in the inset of that figure. There one can see that, if the $T > T_{max}$ values of S_{fit} are scaled with measured $S_m(T > T_{max})$, then $S_{fit} \rightarrow 0$ at $T > 0$ that is not allowed by thermodynamics. Notice that in the inset of Fig. 7, the high temperature value of S_{fit} is referred to $R \ln 2$ because of the scaling procedure. In such scenario, the Nernst postulate imposes $S_m(T) \rightarrow 0$ at $T = 0$, undergoing an inflection point where this sort of 'entropy bottleneck' occurs [18]. This fact indicates that the $C_m(T)/T$ maximum is driven by a thermodynamic constraint instead of classical magnetic interactions effect.

Divergent power laws for the $C_m(T)/T$ dependence are a characteristic of these frustrated systems, because low energy magnetic excitations strongly accumulate at $T \rightarrow 0$. This is due to the fact that no order parameter, able to reduce the GS degeneracy, can develop. Since entropy accumulation cannot exceed the available degrees of freedom provided by the doublet GS, the system is forced into an alternative minimum of the free en-

ergy [20]. Since this transition occurs in a continuous way, no discontinuity (or jump) is observed in $C_m(T)/T$, whilst such a discontinuity is observed in $\partial C_m/\partial T$, i.e. the third derivative of the free energy. Even the faint structure observed in the magnetic susceptibility between 1 and 1.2 K may reveal a competition between two broad minima in the free energy which are blurred out by moderate magnetic field. The origin of such entropy bottleneck can be understood in the context of magnetic frustration of magnetic interactions due to a peculiar geometrical configuration, like the 3D network of corner-sharing triangles presented in Fig. 1, which mimics a trillium flower.

A relatively large paramagnetic Curie-Weiss temperature compared with the corresponding ordering temperature is frequently used to define a frustration parameter: $f = \frac{\theta_p}{T_{ord}}$ [21]. This heuristic criterion reflects the decrease of T_{ord} in respect to the expected values evaluated within a mean field approximation. In the case of CeIrSi, the $\chi(T)$ and $C_m(T)/T$ maxima around 1.3 K are more than one order of magnitude smaller than $\theta_p = -21$ K, revealing a ratio $f > 10$ that hints to a frustration scenario for the magnetic moments.

V. CONCLUSIONS

The peculiar trillium type crystalline structure of CeIrSi provides the possibility to study the effects of magnetic frustration in a 3D Ce-lattice. The entropy driven character of the anomaly, observed around 1.3 K, is deduced from the divergent power law dependence of $C_m(T)/T$. At that temperature, the entropy is constrained to change trajectory in order to not overcome the $S_m = R \ln 2$ limit imposed by the Nernst postulate. Notably, there is a number of compounds showing similar $C_m(T)/T$ anomalies, followed by very similar power law dependencies at higher temperature [18], all of them related to underlying frustration features. The present compound, with trillium type structure, exhibits the same spin-ice character than pyrochlore structured ones, c. f. $\text{Dy}_2\text{Ti}_2\text{O}_7$, suggesting that magnetically frustrated paramagnets slide into an alternative free energy minimum driven by entropy constraints.

The $\rho \propto T^2$ dependence, along the range where $\chi(T)$ and $C_m(T)/T$ maxima show up, reveals that the nature of random interactions occurring in a magnetically frustrated configuration clearly differs from a spin glass scenario. Despite some common features related to disordered interactions, like the effect of magnetic field observed in the $M(T)/H$ and $C_m(T)/T$ dependence around re-

spective maxima may arise, the electron-spin scattering coherence of frustrated systems reveals dis-

tinct differences between dynamic and frozen landscapes.

-
- [1] D. Schiferl; Jour. Chem. Phys. **52** (1970) 3234.
 - [2] R. Moessner and J. T. Chalker; Phys. Rev. B **58** (1998) 12049.
 - [3] Z. Hiroi, K. Matsuhira, M. Ogata; J. Phys. Soc. Japn. **72** 304545 (2003).
 - [4] see for example J.G. Sereni, M. Giovannini, M. G-Berisso, F. Gastaldo; J. Phys.: Condens. Matter **28** (2016) 475601.
 - [5] S.M. Disseler, J.N. Svensson, S.C. Peter, C.P. Byers, C. Baines, A. Amato, S.R. Giblin, P. Carretta, M.J. Graf; arXiv:1110.0118v2 [cond-mat.str-el] (2011).
 - [6] K. Klepp and E. Parthé; Acta Cryst. **38** (1982) 1541.
 - [7] B. Chevalier, P. Lejay, A. Cole, M. Vlasse, J. Etourneau; Sol. State. Commun. **41** (1982) 801.
 - [8] B. Heying, R. Pöttgen, M. Valldor, U.Ch. Rodewald, R. Mishra, R-D. Hoffmann; Monstashefte fuer Chemie **135** (2004) 1335.
 - [9] C.B. Shoemaker, D.P. Shoemaker; Acta Crystallogr. **18** (1965) 900.
 - [10] R. Mishra, R.-D. Hoffmann, R. Pöttgen; Z. Anorg. Allg. Chem. **627** (2001) 1787.
 - [11] J. Evers, G. Oehlinger, A. Weiss, C. Probst; Solid State Commun. **50** (1984) 61.
 - [12] F. Kneidinger, Ph.D. Thesis, Technische Universität Wien (2013), unpublished.
 - [13] A. Szytula M. Hofmann, J. Leciejewicz, B. Penc, A. Zygmunt; J. Alloys Compounds. **316** (2001) 58.
 - [14] H. Yashima, C. Feng lin, T. Satoh, H. Hiroyoshi, K. Kohn; Sol. State Commun. **57** (1986) 793.
 - [15] T.A. Redpath and J.M. Hopkinson; Phys. Rev. B **82** (2010) 014410.
 - [16] J.G. Sereni, P. Pedrazzini, M. Gómez Berisso, A. Chacoma, S. Encina, T. Gruner, N. Caroca-Cananles, C. Geibel; Phys. Rev. B **91** (2015) 174408.
 - [17] H. Michor, J.G. Sereni, M. Giovannini, E. Kampert, L. Salamakha, E. Bauer; Phys. Rev. B **95** (2017) 115146.
 - [18] J.G. Sereni, J. Low Temp. Phys. **179** (2015) 126.
 - [19] J. A. Mydosh, in *Spin Glasses: An Experimental Introduction*, Taylor & Francis, 1993.
 - [20] J.G. Sereni, J. Low Temp. Phys. **190** (2018) 1.
 - [21] A.P. Ramirez, G.P. Espinosa, A.S. Cooper; Phys. Rev. Lett. **64** (1990) 2070.